AN EXPERIMENTAL INVESTIGATION OF TRANSIENT HOT SPOT EFFECTS ON THE HEAT TRANSFER DURING CONVECTIVE BOILING INSIDE MICROCHANNELS

Gustavo Matana Aguiar
Heat Transfer Research Group, Escola de Engenharia de São Carlos (EESC), University of São Paulo (USP), Av. Trabalhador São-Carlense, 400, São Carlos-SP, 13.566-590, Brazil
gustavo.matana.aguiar@usp.br

Débora Carneiro Moreira
Heat Transfer Research Group, Escola de Engenharia de São Carlos (EESC), University of São Paulo (USP), Av. Trabalhador São-Carlense, 400, São Carlos-SP, 13.566-590, Brazil
dcmoreira@id.uff.br

Gherhardt Ribatski
Heat Transfer Research Group, Escola de Engenharia de São Carlos (EESC), University of São Paulo (USP), Av. Trabalhador São-Carlense, 400, São Carlos-SP, 13.566-590, Brazil
ribatski@sc.usp.br

Abstract. *The effect of hot spots on the heat removal efficiency during flow boiling in micro-scale channels is still an open issue in the literature. Despite of its importance, this subject has attracted the attention of only few authors, especially regarding flow boiling in single-channels. In this context, the present study concerns an experimental investigation on the effects of local high heat fluxes on convective boiling in a micro-scale channel of 1.1 mm ID for HFC-134a, saturation temperature of 33°C and mass velocity of 1600 kg/m²s. The hot spot is a segment of the test section 10 mm long in between two segments 40 mm long. Experimental results were obtained, firstly, for a constant heat flux of 80 kW/m² at the hot spot and a background heat flux of 40 kW/m² for the regions of the test section upstream and downstream of the hot spot. Then, experiments were performed for pulsating heat fluxes at the hot spot, varying sinusoidally with amplitude ranging from 5 to 20 kW/m², frequencies of 0.5 Hz and 1 Hz and a fixed RMS value of 80 kW/m². The transient behavior of the heat transfer coefficient was evaluated at the hot spot and also at its upstream and downstream regions. It was found that the amplitude of the oscillation of the heat transfer coefficient at the hot spot increases with an increment in amplitude of the heat flux oscillation. Moreover, the heat transfer coefficient and the heat flux oscillate at the same frequency. During transient tests, it was observed that the heat transfer coefficient at the region upstream the hot spot increases with varying the heat flux at the hot spot. However, this augmentation was within the range of uncertainty of the heat transfer coefficient measurements.*

Keywords: Convective boiling, Microchannels, Hot spot, Transient

1. INTRODUCTION

According to Kandlikar (2005), the heat flux dissipated by late integrated circuits (ICs) can easily reach 1 MW/m², exceeding the current limit of air-cooling technology and thus demanding new cooling technologies to cope with the high heat flux dissipation. As noted by Mudawar et al. (2013), the challenge of dissipating extremely high heat fluxes is not only limited to applications such as computer chips, but similar demands emerged in early 1990s on devices such as solar concentrators, nuclear reactors, particle accelerators, fuel cells and radars. Agostini et al. (2007) performed an extensive literature review comparing different cooling technologies and concluded that two-phase flow boiling in microchannels was the most promising technique at that moment. The increase in heat removal efficiency by microscale channels, when compared to macroscale, is partially explained by the larger ratio of wetted area per volume. In addition, when convective boiling is the heat transfer mechanism, the efficiency is further increased when compared to single-phase cooling.

The main difficult encountered when employing flow boiling in microchannels for cooling is the relatively limited understanding of two-phase transport behavior at small scales (Mudawar, 2013). The prediction of the heat transfer coefficient relies almost entirely on empirical correlations, usually valid only for a range of operational conditions. Also, during boiling in microchannels, undesirable effects of thermal instabilities that can cause severe pressure oscillations are present. Another issue that remains unclear to microchannel cooling technology is the effect of local high heat flux regions (hot spots) on the system performance (Bogojevic et al., 2011). It is well known that heat dissipation on CPUs is non-uniform, thus the mitigation of hot spots is an important aspect to be considered in the design of thermal management devices (Hamman et al., 2007). In solar concentrators and photovoltaic cells, the solar

cell cooling scheme has to deal with the presence of hot spots, which greatly affects the energy conversion efficiency as reported by Baig et al. (2012). Additionally, hot spots may eventually lead to harmful consequences such as the device burnout. Therefore, it is essential to investigate and fully characterize this phenomenon.

Few studies in the literature comprises an investigation of hot spots effects on the cooling performance of heat sinks composed of multiples microchannels (Sharma et al., 2015; Ritchey et al., 2014; Bogojevic et al., 2011; Cho et al. 2010; Kim et al., 2010). According to the best of the present authors' knowledge, solely Miler et al. (2010) investigated the effects of transient hot spot on the heat transfer during flow boiling for single microscale channels, with focus on the effects of pulsed heating in governing physics of bubble nucleation. In this context, the present work concerns an experimental investigation on the effects of non-uniform heating during convective boiling in small diameter channels. The experiments were performed for a horizontal stainless steel channel (AISI-304) with an internal diameter of 1.1 mm and outer diameter of 1.3 mm, using HFC-134a as refrigerant.

2. EXPERIMENTAL APPARATUS

The experimental setup, shown in Fig. 1, is composed of the main circuit containing the test fluid and an auxiliary water circuit. The auxiliary circuit is used to control the saturation pressure in the main circuit (ii), to subcool the refrigerant entering the micropump (iii) and the pre-heater (iv) and to condense and subcool the test fluid in the condenser (i).
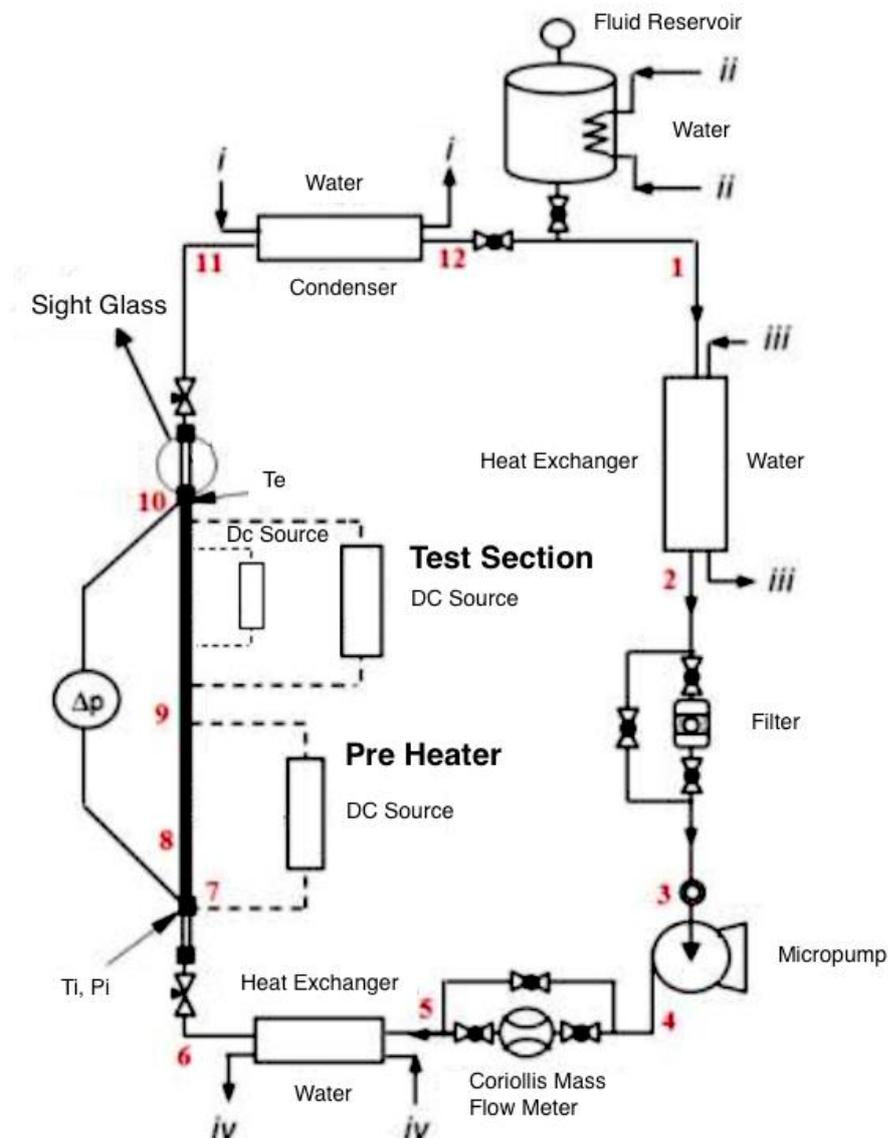
Figure 1. Schematic diagram of main circuit

In the main circuit, a self-lubricating oil-free micropump drives the refrigerant. A mass flow meter operating by the Coriollis principle is placed downstream of the micropump. The mass flow is set by an automatic PI control system acting on a variable-frequency drive that powers the pump. An absolute pressure transducer and a thermocouple immersed within the fluid, both located at the pre-heater entry, are used to evaluate the thermodynamic state of the refrigerant at the pre-heater inlet. Needle valves placed upstream of pre-heater and downstream of the test section are used to minimize two-phase flow oscillations due to the confined bubble formation. Also, two transparent quartz tubes of 1.0 mm internal diameter and 100 mm long are installed upstream the pre-heater and downstream the test section. The first visualization section is used to check the presence of vapor bubbles at the pre-heater inlet, while at the second tube, flow patterns are visualized. The pre-heater and the test section are 355 and 90 mm long, respectively, and formed by a 495 mm straight horizontal stainless steel single tube, as illustrated in Fig. 2.
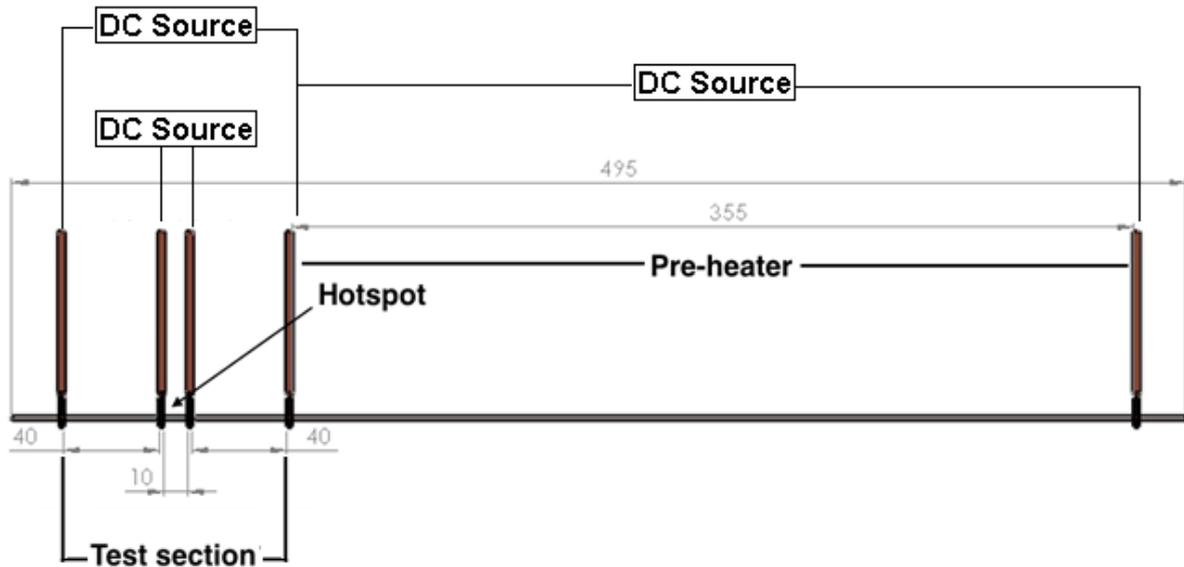
Figure 2. Schematic diagram of the pre-heater and test section (Dimensions in mm).

The test section is composed of a single tube containing a 10 mm long hot spot section, which is located in between two 40 mm long tube segments, as shown in Fig. 3. The heating effect at the tube is obtained through Joule effect by directly powering its surface. One DC power source powers the pre-heater, while two DC power sources supply electrical current to the test section. As shown in Fig. 2, one of them is connected to the external terminals and powers uniformly all the test section length. The second one powers only the hot spot, delivering extra heat to this region. The DC source powering the hot spot is controlled analogically and is able to deliver sinusoidal, saw tooth, square and triangle power waves by means of a LabView script, which acts as a function generator. A differential pressure transducer with its pressure taps installed at the pre-heater entry and at the test section exit measures the total pressure drop along the microchannel.
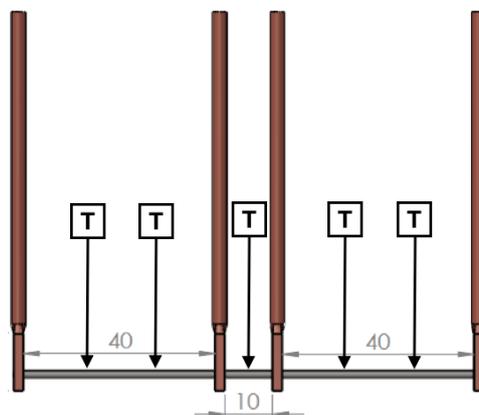
Figure 3. Schematic diagram of the test section

For transient temperature measurements at the hot spot section, a type K thermocouple composed of wires with diameter of 0.0005' is used. At the remaining sections, four pairs of type K thermocouples made of wires with diameters of 0.003' are placed 15 mm apart from the electrodes. A thermal adhesive made of alumina oxide and boron nitride (Arctic Alumina™) that provides good thermal contact and electrical insulation, fixes all the thermocouples. Thermocouples were calibrated using a thermostatic bath and the uncertainty was estimated according to the procedure suggested by Abernethy and Thompson (1973). The method of sequential perturbation according to Taylor and Kuyatt (1994) was employed to calculate the uncertainty associated to derived parameters. The experimental accuracy of measured and derived parameters is summarized in Tab. 1. In order to minimize heat losses to the environment, the pre-heater and test section are covered with consecutive layers of rock wool and elastomeric foam. The signals from the transducers are gathered and recorded by a National Instruments data acquisition system (SCXI-1000) and the data reduction procedure was implemented through a code using Matlab. The experimental data points were acquired during a period of 5 seconds with a recording frequency of 100 data per second.

Table 1. Uncertainties of measured and derived parameters.

Tube Internal Diameter	20 μm
$L_{hot\ spot}$	0.1 mm
P	4.5 kPa
ΔP	150 Pa
T	0.15 °C
$\dot{m}$	0.1 %
q"	5 %
HTC	9 %

3. DATA REDUCTION

The mass velocity G is calculated as the ratio between the mass flow rate $\dot{m}$ and the internal cross sectional area of the tube as follows:

$$G = \frac{4\dot{m}}{\pi D_{int}{}^2} \tag{1}$$

where D_{int} is the tube internal diameter.

A one-dimensional model was built to evaluate the properties of the test fluid along the microchannel. In this model, the microchannel is discretized according to 5061 discrete elements. Figure 4 shows a schematic of each discrete element. The data regression procedure assumes (i) one-dimensional flow in the axial direction of the tube, (ii) negligible heat losses, (iii) uniform heating, (iv) negligible gravitational pressure drop, (v) constant pressure gradient along each discrete element and (vi) uniform length of discrete elements.
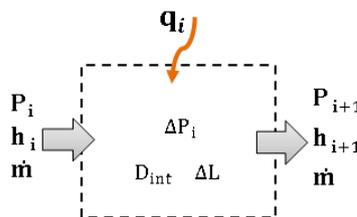
Figure 4. Infinitesimal discrete elements adopted in the data reduction procedure

Energy balance gives the fluid enthalpy h_{i+1} at the exit of each discrete element as follows:

$$h_{i+1} = h_i + \frac{q^{"}{}_i \pi D_{int} \Delta L}{\dot{m}} \tag{2}$$

where $q^{"}{}_i$ is the local heat flux applied by the DC source and ΔL is the discrete element length.

For the single-phase region, the pressure drop along each infinitesimal element and the pressure at its exit, P_{i+1}, was calculated based on the correlation of Churchill (1977) to evaluate the Fanning friction factor f_i for a smooth tube. The pressure at the exit of each discrete element is given as follows:

$$P_{i+1} = P_i - \frac{2 f_i G^2}{D_{int} \rho_i} \Delta L \tag{3}$$

where ρ_i is the local fluid density.

The data reduction was performed using a Matlab (2014b) code with the thermodynamic and transport properties of the fluid evaluated according to CoolProp (V4.0). The transition from single-phase to two-phase flow occurring in the pre-heater and the single-phase length were characterized at the discrete element at which the fluid enthalpy estimated according to Eq. (2) becomes higher than the saturation enthalpy of the liquid at the local pressure. The pressure drop gradient along the two-phase region $\frac{dP}{dz}_{2\emptyset}$ is given as the ratio of the pressure drop difference between the measured total pressure drop along microchannel $\Delta P_{measured}$ and single-phase region $\Delta P_{single-phase}$ and the corresponding two-phase region tube length $L_{2\emptyset}$, as follows:

$$\frac{dP}{dz}_{2\emptyset} = \frac{\Delta P_{measured} - \Delta P_{single-phase}}{L_{2\emptyset}} \tag{4}$$

The pressure at the end of the test section P_{exit} is given by subtracting the total pressure drop measured by a differential transducer $\Delta P_{measured}$ from the absolute pressure at the pre-heater inlet, P_{entry}, measured by an absolute pressure transducer, as follows:

$$P_{exit} = P_{entry} - \Delta P_{measured} \tag{5}$$

The local vapor quality in the two-phase region is estimated from local pressure and enthalpy. The internal wall temperatures $T_{w,int}$ at each of the five cross-sections are obtained through the solution of the heat diffusion equation considering one-dimensional conduction through the tube wall, uniform volumetric heat generation $\dot{q}$ (due to Joule effect) and known external wall temperatures, as follows:

$$T_{w,int} = T_{w,ext} + \frac{\dot{q}}{4k} \frac{\left(D_{ext}^2 - D_{int}^2\right)}{4} - \frac{\dot{q}}{2k} \frac{D_{ext}^2}{4} \ln\left(\frac{D_{ext}}{D_{int}}\right) \tag{6}$$

where the external tube wall temperature $T_{w,ext}$ is the average temperature between the two thermocouples placed at the corresponding cross-section and k is the thermal conductivity of the tube.

The heat losses to the ambient $\dot{Q}_{losses}$ were estimated by powering the pre-heater and the test section with uniform heat flux while maintaining vacuum inside the microchannel. Then, when steady state is achieved, it is assumed that the power supplied to the tube corresponds to the heat losses dissipated to the environment. Figure 5 shows a plot of heat losses vs. temperature differences between tube wall and room temperatures. The wall temperature is evaluated as the average temperature given by the thermocouples along the tube. This figure also presents the curve fitting of the heat losses data used in the data regression procedure.

The delivered electrical power by each DC source takes into account the losses in cable extensions and contact resistance between electrodes and tube. The effective heat generated $\dot{Q}_{effective}$ by each DC source is estimated as the delivered electrical power VI minus the heat loss parcel corresponding to the fraction of the tube length powered by the DC source, as follows:

$$\dot{Q}_{effective} = VI - \frac{L_{heated}}{L_{total}} \dot{Q}_{losses} \tag{7}$$

The heat flux q'' is calculated as the ratio of the effective heat delivered by the DC source to the fluid and the heated area, as follows:

$$q'' = \frac{\dot{Q}_{effective}}{\pi D_{int} L_{heated}} \tag{8}$$
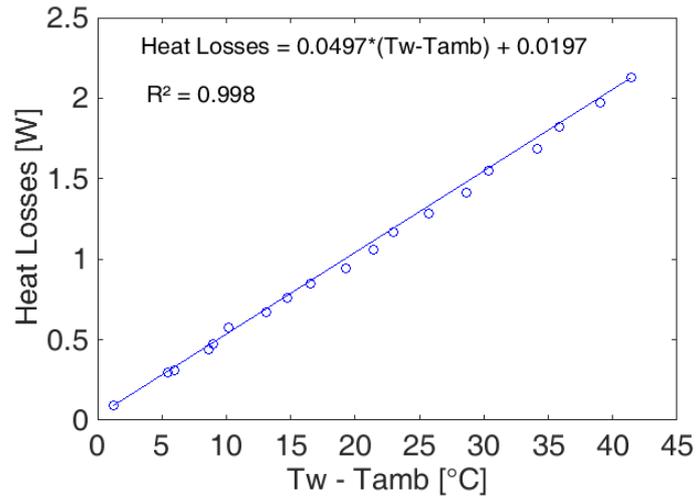
Figure 5. Variation of heat losses with increasing temperature differences between the tube wall and the environment.

The local heat transfer coefficient is given as follows:

$$h = \frac{q''}{(T_{w,int} - T_{fluid})} \tag{9}$$

where the fluid temperature T_{fluid} is estimated from the local saturation pressure.

4. RESULTS

The heat transfer coefficient was evaluated at the test section using HFC-134a as the working fluid, a mass velocity of 1600 kg/m²s and saturation temperature of 33 °C. Initially, steady state experiments were performed by imposing a heat flux of 35 kW/m² at the pre-heater, 40 kW/m² at the regions of the test section upstream and downstream of the hot spot and 80 kW/m² at the hot spot, as illustrated in Fig. 6. For the transient experiments, the heat fluxes at the pre-heater and test section were maintained, while the heat flux at the hot spot was varied sinusoidally with a fixed RMS value of 80 kW/m², amplitudes of 5, 10, 15 and 20 kW/m² and frequencies of 0.5 and 1 Hz. For all test conditions, a time-averaged vapor quality of 0.14 was maintained at the hot spot region.
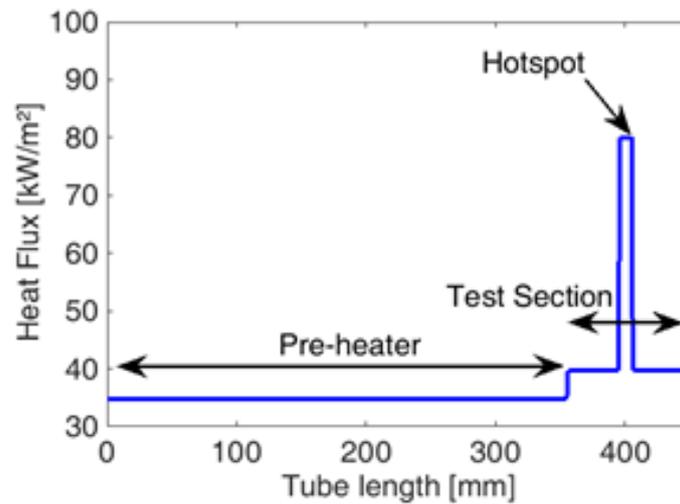
Figure 6. Heat flux profile at the pre-heater and test section for the steady state experiments.

Figures 7 and 8 compare the heat transfer coefficient at the hot spot under steady state and transient conditions for pulsating frequencies of 0.5 and 1 Hz, respectively. The heat transfer coefficient signals for each tested frequency were manually synchronized to match peak values. It can be seen in these figures that the oscillation frequency of the heat flux and heat transfer coefficient are the same. Moreover, an increase in the amplitude of the oscillating heat flux is followed by an increase in amplitude of heat transfer coefficient. Also, the time-averaged heat transfer coefficient is almost independent of the heat flux amplitudes and frequencies, since the variation of its RMS value is lower than 1% for the experimental conditions evaluated in the present study.
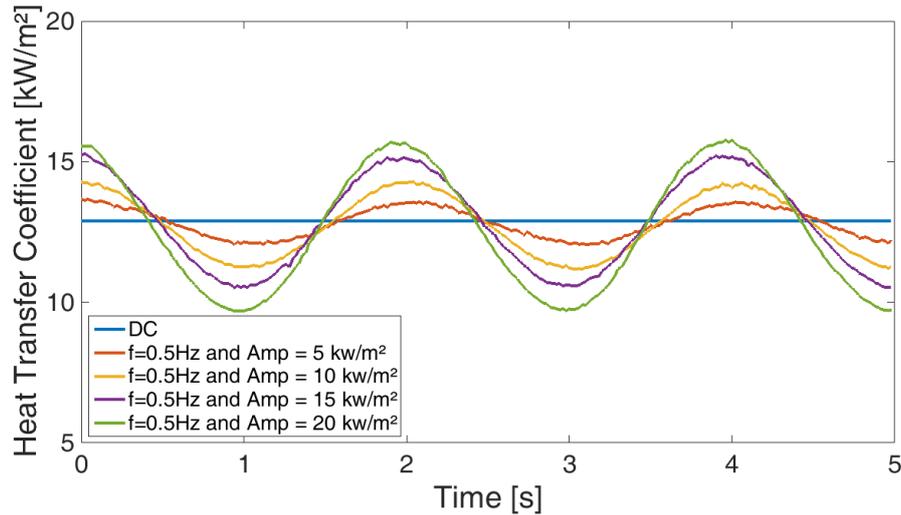
Figure 7. Transient behavior of the heat transfer coefficient during convective boiling in the hot spot region for a pulsating frequency of 0.5 Hz and amplitudes ranging from 0 to 20 kW/m².
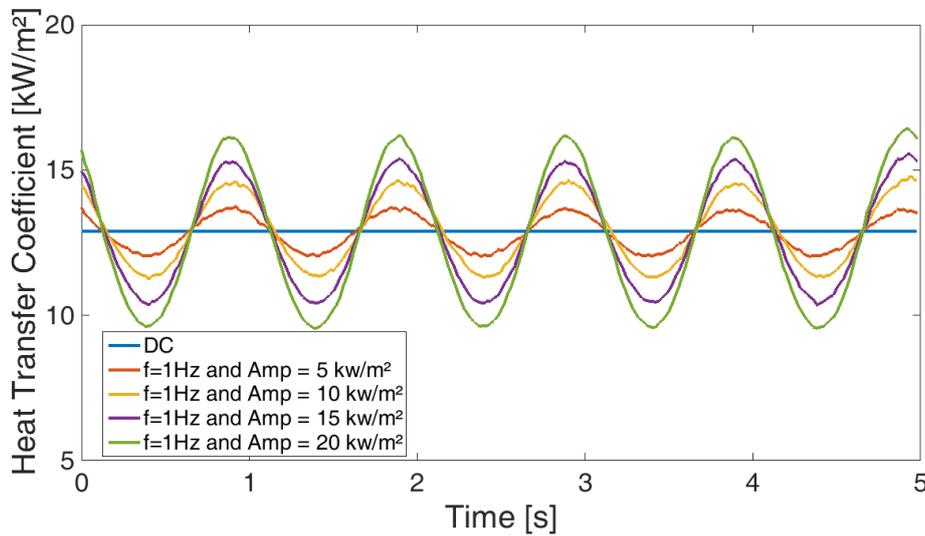
Figure 8. Transient behavior of the heat transfer coefficient during convective boiling in the hot spot region for a pulsating frequency of 1.0 Hz and amplitudes ranging from 0 to 20 kW/m².

The dynamic behavior of the heat transfer coefficient upstream and downstream of the hot spot are shown in Figs. 9 and 10, respectively. A moving average filter was used to smooth the curves. In these figures, oscillations with the same frequency than the imposed heat flux and amplitudes of the order of 1% of the average value of the heat transfer coefficient are observed. Moreover, it seems that the amplitude of the heat flux oscillation at the hot spot does not affect the amplitude of the oscillations of the heat transfer coefficient downstream and upstream the hot spot. Contrary to the region downstream of the hot spot, according to Fig. 10, the upstream heat transfer coefficient tends to oscillate around an average value slightly greater than the average heat transfer coefficient corresponding to the data obtained for steady heat flux. Similar behaviors to those displayed in Figs. 9 and 10 were observed for heat flux oscillations according to a frequency of 1Hz.
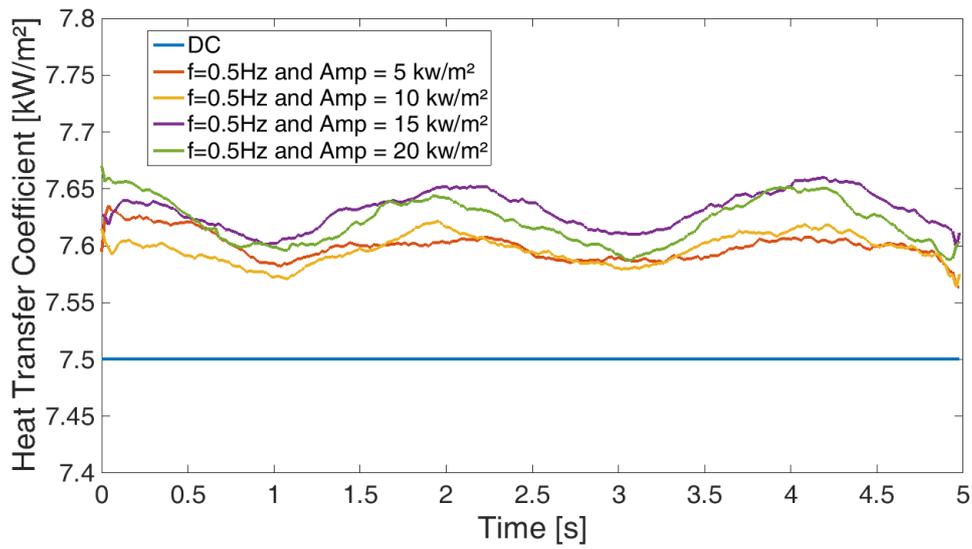
Figure 9. Transient behavior of the heat transfer coefficient during convective boiling in the region upstream of the hot spot for a pulsating frequency of 0.5 Hz.
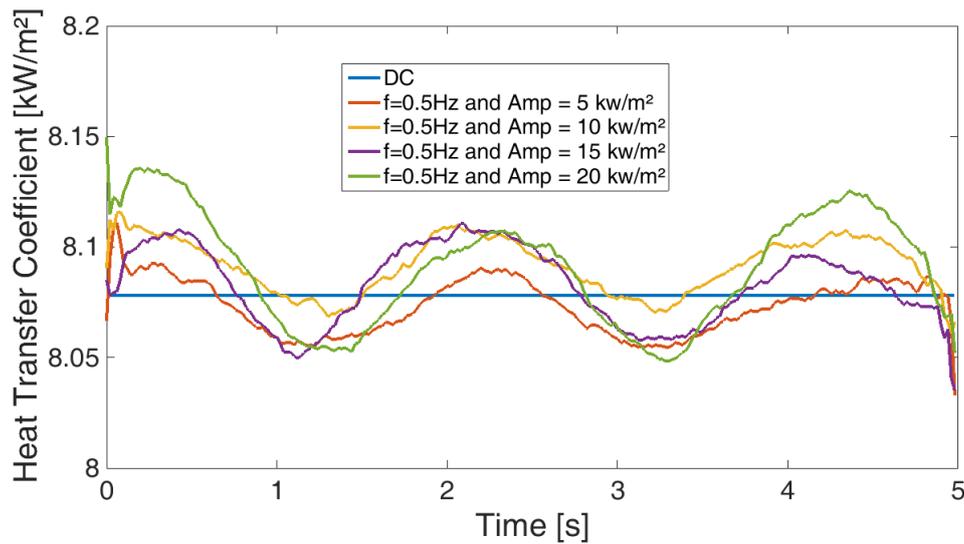
Figure 10. Transient behavior of the heat transfer coefficient during convective boiling in the region downstream of the hot spot region for a pulsating frequency of 0.5 Hz.

5. CONCLUSIONS

Based on the analysis of the experimental data obtained in the present study, the following conclusions can be drawn for tested conditions:

- The heat transfer coefficient and the heat flux at the hot spot oscillate at the same frequency;
- At the hot spot, the amplitude of the oscillation of the heat transfer coefficient rises with an increase in the amplitude of the heat flux oscillation;
- The RMS value of the heat transfer coefficient for oscillating conditions is similar to the heat transfer coefficient for steady heat flux, independently of the frequency and the amplitude of the applied heat flux;
- For variable heat flux at the hot spot, the upstream heat transfer coefficient oscillates around a mean value slightly greater than the corresponding value for steady heat flux.

6. ACKNOWLEDGEMENTS

7. REFERENCES

Abernethy, R.B., Thompson, J.W., 1973. *Handbook of uncertainty in gas turbine measurements*. Air Force Systems Command, Arnold Engineering Development Center.

Agostini, B., Fabbri, M., Park, J.E., Wojtan, L., Thome, J.R., Michel, B., 2007. "State of the Art of High Heat Flux Cooling Technologies". *Heat Transfer Engineering*, Vol. 28, n. 4, p. 258–281.

Baig, H., Heasman, K.C., Mallick, T.K., 2012. "Non-uniform illumination in concentrating solar cells". *Renewable and Sustainable Energy Reviews*, Vol. 16, n. 8, p. 5890–5909.

Bell, I.H., Wronski, J., Quoilin, S., Lemort, V., 2014. "Pure and pseudo-pure fluid thermophysical property evaluation and the open-source thermophysical property library CoolProp". *Industrial & Engineering Chemistry Research*, Vol. 53, n. 6, p. 2498-2508.

Cho, E.S., Choi, J.W., Yoon, J.S., Kim, M.S., 2010. "Experimental study on microchannel heat sinks considering mass flow distribution with non-uniform heat flux conditions". *International Journal of Heat and Mass Transfer*, Vol. 53, n. 9-10, p. 2159–2168.

Churchill, S.W., 1977. "Friction-factor equation spans all fluid-flow regimes." *Chemical engineering*, Vol. 84, n. 24, p. 91-92.

Hamann, H.F., Weger, A., Lacey, J.A., Hu, Z., Bose, P., Cohen, E., Wakil, J., 2007. "Hotspot-limited microprocessors: Direct temperature and power distribution measurements". *IEEE Journal of Solid-State Circuits*, Vol. 42, n.1, p. 56–64.

Kandlikar, S.G., 2005. "High Flux Heat Removal with Microchannels—A Roadmap of Challenges and Opportunities". *Heat Transfer Engineering*, Vol. 26, n. 8, p. 5–14.

Kim, Y.J., Joshi, Y.K., Fedorov, A.G., Lee, Y.J., Lim, S.K., 2010. "Thermal Characterization of Interlayer Microfluidic Cooling of Three-Dimensional Integrated Circuits With Nonuniform Heat Flux". *Journal of Heat Transfer*, Vol. 132, n. 4, p. 041009.

MATLAB 2014b , The MathWorks, Inc., Natick, Massachusetts, United States.

Miler, J.L., Flynn, R., Refai-Ahmed, G., Touzelbaev, M., David, M., Steinbrenner, J., Goodson, K.E., 2010. "Effects of transient heating on two-phase flow response in microchannel heat exchangers". In *Proceedings of the ASME InterPack Conference 2009*. San Francisco, U.S.A.

Mudawar, I., 2013. "Recent Advances in High-Flux, Two-Phase Thermal Management". *Journal of Thermal Science and Engineering Applications*, Vol. 5, n. 2, p. 021012.

Ritchey, S.N., Weibel, J.A., Garimella, S.V., 2014. "Effects of Non-Uniform Heating on the Location and Magnitude of Critical Heat Flux in a Microchannel Heat Sink". *International Journal of Micro-Nano Scale Transport*, Vol. 5, n. 3, p. 95–108.

Sharma, C.S., Schlottig, G., Brunschwiler, T., Tiwari, M.K., Michel, B., Poulikakos, D., 2015. "A novel method of energy efficient hotspot-targeted embedded liquid cooling for electronics: An experimental study". *International Journal of Heat and Mass Transfer*, Vol. 88, p. 684–694.

Taylor, B.N., Kuyatt, C.E., 1995. "Guidelines for evaluating and expressing the uncertainty of NIST measurement results". US Department of Commerce, National Institute of Standards and Technology.

8. RESPONSIBILITY NOTICE

The authors are the only responsible for the printed material included in this paper.